

Overtone Spectroscopy of Sulfonic Acid Derivatives

Joseph R. Lane and Henrik G. Kjaergaard*

Department of Chemistry, University of Otago, P.O. Box 56, Dunedin, New Zealand

Kathryn L. Plath and Veronica Vaida

Department of Chemistry and Biochemistry and CIRES, University of Colorado, Campus Box 215, Boulder, Colorado 80309

Received: December 21, 2006; In Final Form: April 5, 2007

Vapor-phase OH-stretching overtone spectra of methanesulfonic acid and trifluoromethanesulfonic acid were recorded in the $\Delta\nu_{\text{OH}} = 4$ and 5 regions using cavity ring-down spectroscopy. We compare these spectra to those of sulfuric acid to consider the effect on vibrational overtone spectra of replacing one of the OH groups with a more or less electronegative group. We complement our experimental work with anharmonic oscillator local mode calculations of the OH-stretching frequencies and intensities. The presence of a weak intramolecular interaction between the hydrogen atom of the OH group and the oxygen atom of the adjacent S=O group in methanesulfonic acid lowers its OH-stretching frequency from what would otherwise be predicted based on the electronegativity of the methyl group.

Introduction

Sulfuric acid (H_2SO_4) and to a lesser extent methanesulfonic acid ($\text{CH}_3\text{SO}_3\text{H}$), produced by atmospheric oxidation of dimethylsulfide (CH_3SCH_3), are involved in important atmospheric processes such as aerosol formation and acid rain.^{1–5} Interest in H_2SO_4 and $\text{CH}_3\text{SO}_3\text{H}$ has increased with the understanding that these oxidized sulfur compounds are an important component of aerosols and therefore have a significant effect on climate.⁶ Large variations in H_2SO_4 and $\text{CH}_3\text{SO}_3\text{H}$ budgets between model simulations and observations are attributed to the incomplete understanding of reaction mechanisms used in parametrized schemes.^{7,8} The pursuit of such fundamental information relevant to aerosol processes was an impetus for studying the series of H_2SO_4 , $\text{CH}_3\text{SO}_3\text{H}$, and trifluoromethanesulfonic acid ($\text{CF}_3\text{SO}_3\text{H}$).

The infrared spectrum of $\text{CH}_3\text{SO}_3\text{H}$ has been previously recorded in the vapor phase,^{9–11} liquid phase,⁹ and in an Ar matrix.¹² In addition, the molecular structure of $\text{CH}_3\text{SO}_3\text{H}$ at aqueous solution surfaces has been probed using vibrational sum frequency spectroscopy.¹³ Previous investigations have focused on changes in the absorption spectra between the liquid, vapor, and saturated vapor phases. Hydrogen bonding has been identified as an important intermolecular interaction that provides structural stability to methanesulfonic acid in both the liquid and saturated vapor phases.¹⁴ A range of theoretical calculations have also been performed on $\text{CH}_3\text{SO}_3\text{H}$, $\text{CH}_3\text{SO}_3\text{H}$ dimer, and monohydrated $\text{CH}_3\text{SO}_3\text{H}$ ($\text{CH}_3\text{SO}_3\text{H}\cdot\text{H}_2\text{O}$) at the Hartree–Fock, MP2, and B3LYP levels of theory.^{14–16}

The infrared spectrum of $\text{CF}_3\text{SO}_3\text{H}$ has been previously recorded in the vapor phase, liquid phase and in an Ar matrix.^{17,18} These infrared spectra, obtained under different experimental conditions, reveal the presence of both monomer and complexed features. $\text{CF}_3\text{SO}_3\text{H}$ is thought to form strong intermolecular hydrogen bonds in both the liquid and saturated

vapor phase.¹⁸ The molecular structure of $\text{CF}_3\text{SO}_3\text{H}$ has been studied by electron diffraction and X-ray crystallography.^{19,20} Previous ab initio studies of $\text{CF}_3\text{SO}_3\text{H}$ were at the MP2, B3LYP, and B88-LYP levels of theory with small basis sets.^{21,22}

The atmospheric importance of H_2SO_4 has led to numerous experimental and theoretical investigations. Low-resolution vapor-phase infrared spectra of H_2SO_4 were recorded as early as the 1960s.^{23,24} More recently, high-resolution vapor-phase spectra in the infrared and near-infrared have been recorded.^{25–27} The OH-stretching overtone-induced dehydration of H_2SO_4 in the stratosphere has been identified as an important process in the generation of spring time sulfate aerosols.^{4,5,28,29} Subsequently, the overtone spectra were recorded in the $\Delta\nu_{\text{OH}} = 4$ and 5 regions to obtain measured absorption intensities in the visible region at energies near the barrier to this vibrationally mediated photochemistry.³⁰ Very recently, the dynamics of this overtone-induced dehydration for H_2SO_4 and $\text{H}_2\text{SO}_4\cdot\text{H}_2\text{O}$ have been investigated by classical trajectory simulations.²⁹ The molecular structure of H_2SO_4 in the gas phase has been determined by microwave spectroscopy.³¹ There have been several theoretical studies of H_2SO_4 at the Hartree–Fock, MP2, B3LYP, and QCISD levels of theory.^{4,25,26,32}

In this work, we investigate the spectroscopic effect of the substituent electronegativity using vibrational overtone spectra of sulfonic acid ($\text{R}-\text{SO}_2-\text{OH}$) derivatives. As the electronegativity of the substituent R increases ($\text{CH}_3 < \text{OH} < \text{CF}_3$), the amount of electron back-donation from the oxygens to the sulfur increases. This effect has been previously observed from the increasing fundamental S=O and S–O stretching wavenumbers with increasing electronegativity of the substituent.^{9,18,23} An increase in the electronegativity of R is also thought to decrease the OH-stretching frequency, although this trend has not been shown clearly.⁹ In the fundamental region, the observed OH-stretching wavenumber of $\text{CH}_3\text{SO}_3\text{H}$ and H_2SO_4 is essentially the same ($\sim 3609\text{ cm}^{-1}$), with that of $\text{CF}_3\text{SO}_3\text{H}$ approximately 25 cm^{-1} lower in energy (3585 cm^{-1}).^{11,18,25} Overtone spectra are very sensitive to bond properties and can be used to study

* To whom correspondence should be addressed. E-mail: henrik@alkali.otago.ac.nz. Fax: 64-3-479-7906. Phone: 64-3-479-5378.

subtle effects in molecular structure and molecular conformation.³³ As higher regions of the potential are probed, even small differences in frequency and anharmonicity of the potential become apparent.

We have used cavity ring-down spectroscopy to measure the vapor-phase OH-stretching overtone spectra of CH₃SO₃H and CF₃SO₃H in the $\Delta\nu_{\text{OH}} = 4$ and 5 regions. Both of these compounds have low vapor pressure at room temperature and are extremely corrosive, making them difficult to handle. In a recent experimental study, Feierabend et al. used cavity ring-down spectroscopy to record OH-stretching overtone spectra of sulfuric acid and we compare our data with these spectra.³⁰ Comparison of the spectra of these three compounds allows us to investigate the effect of a more (R = CF₃) or less (R = CH₃) electronegative substituent on the OH-stretching overtone spectra.

We have calculated the OH-stretching transitions of CH₃SO₃H, H₂SO₄, and CF₃SO₃H to facilitate spectral interpretation. We use an anharmonic oscillator local mode model with dipole moment functions obtained from ab initio coupled cluster calculations. The local mode model was developed in the 1970s to describe the highly excited vibrational states of molecules.³⁴ Since then it has been successfully used in the description and analysis of XH-stretching overtone spectra (where X = C, N, O, etc.).^{35–39} More recently, it has been used to calculate relative and absolute intensities of CH- and OH-stretching overtone transitions to high accuracy, often within experimental error.^{40–43}

Experimental Section

The spectra of methanesulfonic and trifluoromethanesulfonic acids were obtained using a pulsed cavity ring-down spectrometer that was described previously^{30,44} to complement the lower energy FTIR spectra in the literature.^{11,18,25} The samples, CH₃SO₃H (Aldrich, $\geq 99.5\%$) and CF₃SO₃H (Aldrich, 98%), were used as received from the manufacturer. Because of the corrosive nature of both acids, modifications were made to the original cell.^{30,44} CH₃SO₃H was measured in a glass cell with Teflon fittings to keep the acid from reacting with any available metal. The increased reactivity and higher vapor pressure of CF₃SO₃H made it more difficult to handle and required building another cell made of Teflon. This Teflon cell is 79 cm long and fits with the same mirror mounts as the original glass cell.^{30,44} The cell consists of 1/2 in. inner diameter Teflon tubing connected by Teflon tee junctions with a 5/8 in. port on each end. The Teflon cell rests snugly inside a copper sheath for a more stable and consistent temperature.

Both the glass and Teflon cells were wrapped in heating tape to allow for easy heating and temperature control. The heating system was calibrated by inserting a thermocouple into the cell and measuring the internal temperature under experimental conditions. CH₃SO₃H and CF₃SO₃H are hygroscopic and have a tendency to form aerosols, which can scatter the laser beam resulting in no signal. To prevent aerosol formation, the compound's vapor pressure was limited by recording at relatively low temperatures with a constant purge gas flow rate. For CH₃SO₃H, we found there to be sufficient number density and negligible aerosol formation to record spectra at 371, 377, and 388 K, which correspond to literature equilibrium vapor pressures of 0.22, 0.32, and 0.63 Torr, respectively.⁴⁵ For CF₃SO₃H, we found additional heating was not required and spectra were recorded at room temperature (294 K) with a literature equilibrium vapor pressure of 1.1 Torr.⁴⁶

In the $\Delta\nu_{\text{OH}} = 4$ region, the mirrors (Los Gatos Research Inc.) have a diameter of 1 in., a 1 m radius of curvature, and a

peak in the reflectivity at 760 nm ($R > 99.997\%$). The base ring-down time constant with these mirrors is 103 μs with the glass cell and 135 μs with the Teflon cell. In the $\Delta\nu_{\text{OH}} = 5$ region, the mirrors (Los Gatos Research Inc.) have a diameter of 1 in. and a 1 m radius of curvature but a peak in the reflectivity at 610 nm ($R > 99.997\%$). The base ring-down time constant with this second set of mirrors is $\sim 100 \mu\text{s}$ with the glass cell. There was no evident change in the observed ring-down time constant over the course of the experiments.

To keep the mirrors clean and free from condensation, a purge gas of helium was introduced directly in front of the mirrors. This slightly reduces the path length of the sample within the cell. A 100 μs ring-down time constant creates an effective path length of approximately 30 km, and the 135 μs ring-down time constant extends the effective path length to 40 km. All of the spectra were obtained using a constant purge flow rate and at local atmospheric pressure (~ 0.8 atm).

The laser used for the absorption experiments was a tunable dye laser (Northern Lights, NL-5-2-MF6) pumped by a frequency doubled Nd:YAG laser (Big Sky). Spectra were recorded with a 0.01 nm resolution ($\sim 0.1 \text{ cm}^{-1}$ for $\Delta\nu_{\text{OH}} = 4$; $\sim 0.2 \text{ cm}^{-1}$ for $\Delta\nu_{\text{OH}} = 5$). The wavelength of the dye laser output was calibrated by comparing a 0.01 nm resolution spectrum of H₂O vapor to published values.⁴⁷ From the manufacturers specifications, the dye laser bandwidth was estimated to be 1 cm^{-1} . The pulse width from the Nd:YAG had a full width at half-maximum (fwhm) of 7 ns. Two dyes were necessary to gather all of the spectra, LDS 751 (range of 720–780 nm) and Kiton Red 620 (range of 585–615 nm). The laser pulses were directed out of the dye laser in an isolator (Newport polarizer, 10GLO8AR.14, and a Newport waveplate, 05RP), then through a 50 cm focusing lens, and directed to two turning mirrors before entering the previously described cells. The beam is focused to a spot size comparable to the low-order transverse electric modes of the optical resonator. Upon leaving the cell, the beam encounters a turning mirror followed by a negative lens (50 cm focal length) and expanded onto the photomultiplier tube (Hamamatsu, R943-02). From the detector, the signal interfaces with the commercially available data acquisition card (Gage Compuscope 1250). The interface software has been described previously.⁴² The card is sampled at 10 MHz for all of these experiments.

Theory and Calculations

The vibrations of OH-stretching oscillators are highly anharmonic and can be described by a simple local mode model.³⁵ If we assume that the OH-stretching vibration is a Morse oscillator, then the vibrational energy levels are given by

$$E(v)/(hc) = \left(v + \frac{1}{2}\right)\tilde{\omega} - \left(v + \frac{1}{2}\right)^2\tilde{\omega}x \quad (1)$$

The Morse oscillator frequency $\tilde{\omega}$ and anharmonicity $\tilde{\omega}x$ are found from the second, third, and fourth order derivatives of the potential energy curve as described previously.^{48,49} These derivatives are found by fitting an eighth order polynomial to a nine point ab initio calculated potential energy curve, obtained by displacing the OH bond from -0.2 to 0.2 \AA in 0.05 \AA steps around equilibrium. This ensures converged derivatives.^{38,50}

The dimensionless oscillator strength f of a transition from the vibrational ground state $|0\rangle$ to a vibrationally excited state $|v\rangle$ is given by^{39,51}

$$f_{v,0} = (4.702 \times 10^{-7} \text{ cm D}^{-2})\tilde{\nu}_{v,0}|\mu_{v,0}|^2 \quad (2)$$

TABLE 1: Selected Geometric Parameters (in Å and deg) of CH₃SO₃H, H₂SO₄, and CF₃SO₃H^a

parameter	CH ₃ SO ₃ H	H ₂ SO ₄	CF ₃ SO ₃ H
R_{OH}	0.9679	0.9689	0.9699
θ_{HOS}	108.2	109.3	109.7
ϕ_{HOSO}	4.6	26.5	18.1
$R_{\text{S-O}}^b$	1.6148	1.5958	1.5935
$R_{\text{S=O(1)}}^c$	1.4373	1.4226	1.4283
$R_{\text{S=O(2)}}^d$	1.4287	1.4226	1.4206
$R_{\text{O}\cdots\text{HO}}$	2.3875	2.4642	2.4596

^a Calculated at the B3LYP/aug-cc-pV(T+d)Z level of theory. ^b Refers to the S–O bond length of the S–OH group(s). ^c Refers to the O atom closest to the OH group. ^d Refers to the O atom furthest to the OH group.

where $\tilde{\nu}_{v_0}$ is the vibrational wavenumber of the transition in cm⁻¹ and $\mu_{v_0} = \langle v|\mu|0\rangle$ is the transition dipole moment matrix element in Debye.

We can expand the transition dipole moment matrix element as

$$\langle v|\mu|0\rangle = \frac{\partial\mu}{\partial q}\langle v|q|0\rangle + \frac{1}{2}\frac{\partial^2\mu}{\partial q^2}\langle v|q^2|0\rangle + \frac{1}{6}\frac{\partial^3\mu}{\partial q^3}\langle v|q^3|0\rangle + \dots \quad (3)$$

where q is the internal vibrational displacement coordinate. The integrals $\langle v|q^n|0\rangle$ required for the transition dipole moment were evaluated analytically.⁵² The dipole moment derivatives required in eq 3 are found from a sixth order polynomial fit to a nine point dipole moment curve calculated over the same range as the potential.

We have optimized the geometry of CH₃SO₃H, H₂SO₄, and CF₃SO₃H using B3LYP hybrid density functional and CCSD(T) ab initio theories. The optimization threshold criteria was set to gradient = 1×10^{-5} au, stepsize = 1×10^{-5} au, energy = 1×10^{-7} au. We have used the Dunning type correlation consistent basis sets supplemented with additional tight d basis functions on sulfur atoms, aug-cc-pV(D+d)Z and aug-cc-pV(T+d)Z.⁵³ These additional tight d functions have been shown to significantly improve the geometries and energies of sulfur-containing compounds.⁵⁴ Normal mode harmonic frequencies were calculated with the B3LYP/aug-cc-pV(T+d)Z method and can be found in the Supporting Information.

The CCSD(T) dipole moment at each geometry was calculated using a finite field approach with a field strength of ± 0.025 au. The single point threshold criteria was set to energy = 1×10^{-8} au, orbital = 1×10^{-8} au, coefficient = 1×10^{-8} au. All calculations were performed with MOLPRO.⁵⁵

Results and Discussion

Calculated Geometries. In Table 1 we compare selected geometric parameters in CH₃SO₃H, H₂SO₄, and CF₃SO₃H calculated with the B3LYP/aug-cc-pV(T+d)Z method. It was not computationally feasible to optimize the geometry of CF₃SO₃H with the CCSD(T)/aug-cc-pV(T+d)Z method. For CH₃SO₃H and H₂SO₄, the results of the B3LYP/aug-cc-pV(T+d)Z optimization are in very good agreement with the CCSD(T)/aug-cc-pV(T+d)Z optimized geometry. The complete B3LYP/aug-cc-pV(T+d)Z, CCSD(T)/aug-cc-pV(D+d)Z, and CCSD(T)/aug-cc-pV(T+d)Z (where available) optimized structures are given in the Supporting Information where we also list the experimental structures.^{19,31}

The B3LYP/aug-cc-pV(T+d)Z optimized geometries of H₂SO₄ and CF₃SO₃H are generally in good agreement with the experimental geometries determined from microwave spectro-

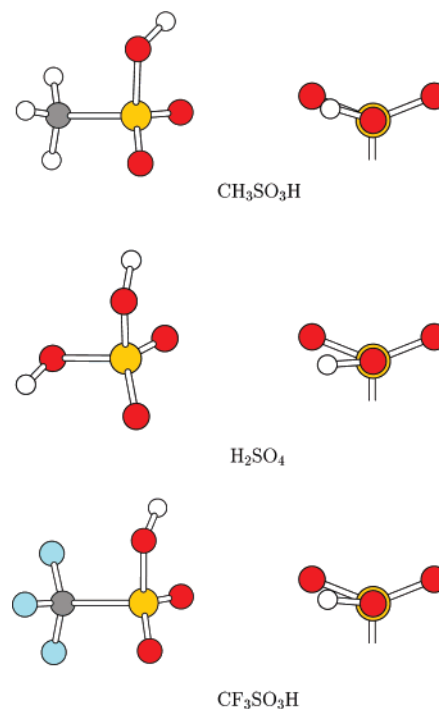


Figure 1. Left: B3LYP/aug-cc-pV(T+d)Z optimized geometry of CH₃SO₃H, H₂SO₄, and CF₃SO₃H. Right: orientation of the OH group looking down the SO–H bond.

copy³¹ and electron diffraction,¹⁹ respectively. However, the CSOH dihedral angle in CF₃SO₃H could not be determined by electron diffraction; so it was fixed to 180°,¹⁹ which is significantly different from our calculated value of $\sim 93^\circ$. We are not aware of any experimental structures of CH₃SO₃H in the literature.

CH₃SO₃H has the longest calculated S=O and S–O bond lengths, followed by H₂SO₄, and finally CF₃SO₃H. This trend supports the concept that as the electronegativity of the substituent increases (CH₃ < OH < CF₃), the amount of electron back-donation from the oxygens to the sulfur increases, and hence the S=O and S–O bond lengths decrease. IR spectra of CH₃SO₃H, H₂SO₄, and CF₃SO₃H have previously been shown to validate this concept, with the S=O and S–O stretching frequencies increasing as the electronegativity of the substituent increases.^{9,18,23}

The effect of the substituent on the OH bond is less obvious than that on the S=O and S–O bonds. As the electronegativity of the substituent increases, the OH bond length increases, with R_{OH} being the shortest in CH₃SO₃H and the longest in CF₃SO₃H. In Figure 1, the orientation of the OH group with respect to the sulfonyl oxygen atoms is shown. In CH₃SO₃H, the dihedral angle between OH and S=O (ϕ_{HOSO}) with the two groups almost aligned is significantly smaller than in H₂SO₄ and CF₃SO₃H. This, in combination with the slightly decreased θ_{HOS} angle, is perhaps a sign of a weak intramolecular interaction between the hydrogen atom of the OH group and the oxygen atom of the adjacent S=O group. The distance between the hydrogen atom of the OH group and the oxygen atom of the closest S=O group (S=O \cdots HO) in CH₃SO₃H is also somewhat shorter than in H₂SO₄ and CF₃SO₃H.

It is not clear why a stronger intramolecular interaction (S=O \cdots HO) is formed in CH₃SO₃H ahead of the other two sulfonic acids. It is possible that the oxygen lone pairs of the OH group interact favorably with the hydrogens of the CH₃ group. CH₃ is also less electronegative than OH and CF₃; hence, in CH₃SO₃H the amount of electron back-donation from the oxygen atoms

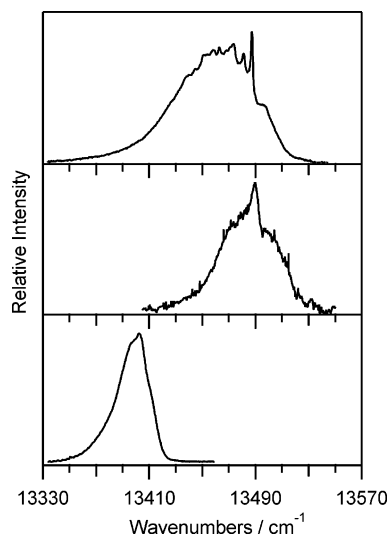


Figure 2. The vapor phase overtone spectra of $\text{CH}_3\text{SO}_3\text{H}$ (top, 388 K), H_2SO_4 (middle, 434 K), and $\text{CF}_3\text{SO}_3\text{H}$ (bottom, 294 K) in the $\Delta\nu_{\text{OH}} = 4$ region. The spectrum of H_2SO_4 is from ref 30.

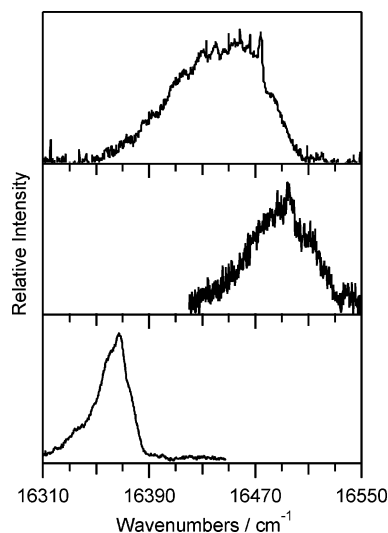


Figure 3. The vapor phase overtone spectra of $\text{CH}_3\text{SO}_3\text{H}$ (top, 388 K), H_2SO_4 (middle, 434 K), and $\text{CF}_3\text{SO}_3\text{H}$ (bottom, 294 K) in the $\Delta\nu_{\text{OH}} = 5$ region. The spectrum of H_2SO_4 is from ref 30.

to the sulfur will be less. This will result in the oxygen atoms of the $\text{S}=\text{O}$ groups in $\text{CH}_3\text{SO}_3\text{H}$ being more electronegative and hence more attractive to the hydrogen atom of the OH group.²³ A natural bond orbital analysis at the B3LYP/AV-(T+d)Z level supports this concept, with the oxygen atom of $\text{CH}_3\text{SO}_3\text{H}$ calculated to be more basic than those of H_2SO_4 and $\text{CF}_3\text{SO}_3\text{H}$.

As seen in Figure 1, the global minimum structure of $\text{CH}_3\text{SO}_3\text{H}$ has C_1 symmetry with the OH group approximately aligned with the adjacent $\text{S}=\text{O}$ group. The energy of the C_s saddle point, with the OH group equidistant from each $\text{S}=\text{O}$ group and the CH_3 group in the plane of symmetry, is calculated to be $\sim 250 \text{ cm}^{-1}$ higher in energy at the B3LYP/avg-cc-pV-(T+d)Z level of theory with one imaginary frequency. For $\text{CF}_3\text{SO}_3\text{H}$, the energy difference between the C_1 global minimum and C_s saddlepoint is $\sim 960 \text{ cm}^{-1}$.

OH-Stretching Transitions. The vapor-phase OH-stretching overtone spectra of $\text{CH}_3\text{SO}_3\text{H}$, H_2SO_4 , and $\text{CF}_3\text{SO}_3\text{H}$ in the $\Delta\nu_{\text{OH}} = 4$ and 5 regions are presented in Figures 2 and 3, respectively. In Table 2, we have tabulated the overtone peak positions, bandwidths, and intensities for these transitions. The

TABLE 2: Observed $\Delta\nu_{\text{OH}} = 4$ and 5 Overtone Peak Positions, Bandwidths (in cm^{-1}), and Oscillator Strengths of $\text{CH}_3\text{SO}_3\text{H}$, H_2SO_4 , and $\text{CF}_3\text{SO}_3\text{H}$

molecule	$\Delta\nu_{\text{OH}} = 4$			$\Delta\nu_{\text{OH}} = 5$		
	$\bar{\nu}$	fwhm	f	$\bar{\nu}$	fwhm	f
$\text{CH}_3\text{SO}_3\text{H}^a$	13 470	55	1.4×10^{-9}	16 453	85	1.3×10^{-10}
H_2SO_4^b	13 490	43	3.3×10^{-9}	16 494	54	2.7×10^{-10}
$\text{CF}_3\text{SO}_3\text{H}^c$	13 403	27	1.3×10^{-10}	16 367	25	1.5×10^{-11}

^a Experimental uncertainties in oscillator strength not including vapor pressure errors are $\pm 0.2 \times 10^{-9}$ and $\pm 0.2 \times 10^{-10}$ for $\Delta\nu_{\text{OH}} = 4$ and 5, respectively. Oscillator strengths measured at 388 K, 0.63 Torr. ^b From ref 30. Uncertainties in oscillator strength are $\pm 0.7 \times 10^{-9}$ and $\pm 0.6 \times 10^{-10}$ for $\Delta\nu_{\text{OH}} = 4$ and 5, respectively. Oscillator strengths measured at 434 K, 1.37 Torr. ^c Experimental uncertainties in oscillator strength not including vapor pressure errors are $\pm 0.3 \times 10^{-11}$ and $\pm 0.4 \times 10^{-12}$ for $\Delta\nu_{\text{OH}} = 4$ and 5, respectively. These intensities are likely low due to an overestimate of the vapor pressure in our cell. See text for details. Oscillator strengths measured at 294 K, 1.1 Torr.

overtone peak positions of $\text{CH}_3\text{SO}_3\text{H}$ were determined by fitting a Lorentzian function to experimental data, and for H_2SO_4 and $\text{CF}_3\text{SO}_3\text{H}$, the clear Q-branch and the experimental band maximum were used, respectively. In both the $\Delta\nu_{\text{OH}} = 4$ and 5 regions, the OH-stretching wavenumber of H_2SO_4 is highest in energy followed by $\text{CH}_3\text{SO}_3\text{H}$ and $\text{CF}_3\text{SO}_3\text{H}$. On the basis of the electronegativity of the substituent, we would have expected the OH-stretch overtones of $\text{CH}_3\text{SO}_3\text{H}$ to lie to the blue of both H_2SO_4 and $\text{CF}_3\text{SO}_3\text{H}$. This is clearly not the case, and we suspect that a weak intramolecular interaction ($\text{S}=\text{O} \cdots \text{HO}$) in $\text{CH}_3\text{SO}_3\text{H}$ to be the cause.

The band profile of the OH-stretching overtones in $\text{CH}_3\text{SO}_3\text{H}$, H_2SO_4 , and $\text{CF}_3\text{SO}_3\text{H}$ has been characterized using the orientation of the transition dipole moment (TDM) to the principal rotation axes.⁵⁶ For $\text{CH}_3\text{SO}_3\text{H}$ and H_2SO_4 , we use the CCSD-(T)/AV(T+d)Z TDM and optimized geometry, for $\text{CF}_3\text{SO}_3\text{H}$ we are limited to the CCSD(T)/AV(D+d)Z results (vide infra). The calculated TDM of the $\Delta\nu_{\text{OH}} = 4$ and 5 OH-stretching transitions in H_2SO_4 approximately bisects the a and c axes, giving rise to a clear Q-branch in the experimental spectra.³⁰ For $\text{CF}_3\text{SO}_3\text{H}$, the calculated TDM of the $\Delta\nu_{\text{OH}} = 4$ and 5 OH-stretching transitions is also more or less in the ac plane but with a small component in the b -axis. This orientation should also give rise to a clear Q-branch in the experimental spectra; however, the greater mass of $\text{CF}_3\text{SO}_3\text{H}$ compared with H_2SO_4 reduces the observed bandwidth, making the Q-branch hard to resolve. The calculated TDM of the $\Delta\nu_{\text{OH}} = 4$ and 5 OH-stretching transitions in $\text{CH}_3\text{SO}_3\text{H}$ is most closely orientated along the a -axis but with significant components in the b and c axes also. From this orientation we would expect to see some form of Q-branch in the experimental spectra, which may explain the sharp feature at the blue edge of the $\Delta\nu_{\text{OH}} = 4$ and 5 OH-stretching transitions in $\text{CH}_3\text{SO}_3\text{H}$.

The observed OH-stretching transitions in $\text{CH}_3\text{SO}_3\text{H}$ are further complicated by the appreciable population of several low-energy OH and CH_3 torsional states.¹² The OH and CH_3 torsional modes in $\text{CH}_3\text{SO}_3\text{H}$ have a fundamental frequency of 203 and 226 cm^{-1} , respectively, producing a symmetric double-well potential. Along this torsional coordinate, the vibrational ground state is approximately 100 cm^{-1} higher in energy than the C_1 global minimum and is below the C_s saddle point, causing a tunneling splitting of this torsional state. We have calculated the ground state tunneling splitting within the Wentzel–Kramers–Brillouin (WKB) approximation using a procedure successfully employed for malonaldehyde and tropolone.^{57,58} We find the ground state tunneling splitting ($T_0 - T_1$) of $\text{CH}_3\text{SO}_3\text{H}$ to be $\sim 5 \text{ cm}^{-1}$. The second vibrational excited state (T_2) along

TABLE 3: Observed and CCSD(T) Calculated OH-Stretching Local Mode Frequencies (in cm^{-1}) of $\text{CH}_3\text{SO}_3\text{H}$, H_2SO_4 , and $\text{CF}_3\text{SO}_3\text{H}$

basis set	$\text{CH}_3\text{SO}_3\text{H}$	H_2SO_4	$\text{CF}_3\text{SO}_3\text{H}$
cc-pV(D+d)Z	3794.8	3789.5	3777.0
aug-cc-pV(D+d)Z	3757.9	3748.4	3736.6
aug-cc-pV(T+d)Z	3784.4	3778.5	
observed ^a	3768.4 ± 2	3763.6 ± 2	3740.8 ± 0.4

^a For $\text{CH}_3\text{SO}_3\text{H}$ and $\text{CF}_3\text{SO}_3\text{H}$, the experimental frequencies are from a Birge–Sponer fit of the $\Delta\nu_{\text{OH}} = 1, 4,$ and 5 transitions. For H_2SO_4 , the experimental frequency is from a Birge–Sponer fit of the $\Delta\nu_{\text{OH}} = 1-5$ transitions. The uncertainty is 1 standard deviation.

this torsional coordinate is likely to be above the C_s saddle point. The $\text{CH}_3\text{SO}_3\text{H}$ spectra were recorded at 377–388 K, hence several torsional states will have an appreciable population. Excitation from these torsional states are not likely to be well resolved, which will increase the apparent bandwidth of the OH-stretching transitions in $\text{CH}_3\text{SO}_3\text{H}$. This is similar to the increased width seen in methyl CH-stretching overtone spectra of, e.g., the xylenes, where the relatively free rotation of the methyl group gives rise to multiple transitions between internal rotational states.⁵⁹ From Figures 2 and 3 it is clear that the bandwidths of the $\Delta\nu_{\text{OH}} = 4$ and 5 OH-stretching transitions in $\text{CH}_3\text{SO}_3\text{H}$ are significantly wider than those for H_2SO_4 and $\text{CF}_3\text{SO}_3\text{H}$.

While the peak position, line shape, and relative intensity can be accurately determined from experiment, the oscillator strengths depend on the accuracy of the vapor pressure. For $\text{CH}_3\text{SO}_3\text{H}$ and $\text{CF}_3\text{SO}_3\text{H}$, vapor pressure data were not available at the temperatures that our spectra were recorded so we have extrapolated using the following equation

$$\ln(P) = A + \frac{B}{T} \quad (4)$$

where T is the temperature in kelvin, A and B are constants obtained by least-squares fitting to the available experimental data. We have used a simple formula for extrapolation as there are limited data points available in the literature. At low temperatures, this equation is likely to slightly overestimate the vapor pressure, while at high temperatures it is likely to slightly underestimate the vapor pressure. This form of extrapolation was used by Tang et al. to fit $\text{CH}_3\text{SO}_3\text{H}$ vapor pressure data measured by droplet evaporation kinetics at 313–328 K and a high-temperature value at 440 K.⁴⁵ The extrapolated vapor pressure of $\text{CH}_3\text{SO}_3\text{H}$ is 0.22, 0.32, and 0.63 Torr at 371, 377, and 388 K, respectively.⁴⁵ For $\text{CF}_3\text{SO}_3\text{H}$, we have extrapolated vapor pressure data measured by ebulliometry at 319–396 K to give a vapor pressure of 1.1 Torr at 294 K.⁴⁶ It is important to note that eq 4 is purely empirical and that the extrapolated vapor pressures possess a large degree of uncertainty.^{45,46} A better defined vapor pressure would allow for a more precise determination of the oscillator strength.

The observed OH-stretching oscillator strength of H_2SO_4 in the $\Delta\nu_{\text{OH}} = 4$ and 5 regions is more than twice that of $\text{CH}_3\text{SO}_3\text{H}$. If we compare the intensity on a per OH oscillator basis, we find the OH-stretching transitions in H_2SO_4 to be 35% and 20% more intense than those of $\text{CH}_3\text{SO}_3\text{H}$ in the $\Delta\nu_{\text{OH}} = 4$ and 5 regions, respectively. The observed oscillator strength of the OH-stretching overtones of $\text{CF}_3\text{SO}_3\text{H}$ in the $\Delta\nu_{\text{OH}} = 4$ and 5 regions is significantly lower than those of $\text{CH}_3\text{SO}_3\text{H}$ and H_2SO_4 . The experimental oscillator strength is dependent on an accurate estimate of the vapor pressure of the sample in our flow cell. There is limited vapor pressure data for $\text{CF}_3\text{SO}_3\text{H}$ in

TABLE 4: Observed and CCSD(T) Calculated OH-Stretching Local Mode Anharmonicities (in cm^{-1}) of $\text{CH}_3\text{SO}_3\text{H}$, H_2SO_4 , and $\text{CF}_3\text{SO}_3\text{H}$

basis set	$\text{CH}_3\text{SO}_3\text{H}$	H_2SO_4	$\text{CF}_3\text{SO}_3\text{H}$
cc-pV(D+d)Z	82.82	83.04	82.83
aug-cc-pV(D+d)Z	85.74	85.88	85.62
aug-cc-pV(T+d)Z	79.57	79.71	
observed ^a	79.8 ± 0.7	77.9 ± 0.7	77.9 ± 0.2

^a For $\text{CH}_3\text{SO}_3\text{H}$ and $\text{CF}_3\text{SO}_3\text{H}$, the experimental anharmonicities are from a Birge–Sponer fit of the $\Delta\nu_{\text{OH}} = 1, 4,$ and 5 transitions. For H_2SO_4 , the experimental anharmonicity is from a Birge–Sponer fit of the $\Delta\nu_{\text{OH}} = 1-5$ transitions. The uncertainty is 1 standard deviation.

TABLE 5: Calculated OH-Stretching Wavenumbers (in cm^{-1}) and Oscillator Strengths of $\text{CH}_3\text{SO}_3\text{H}$, H_2SO_4 , and $\text{CF}_3\text{SO}_3\text{H}$

ν	$\text{CH}_3\text{SO}_3\text{H}^a$		H_2SO_4^a		$\text{CF}_3\text{SO}_3\text{H}^b$	
	$\tilde{\nu}$	f	$\tilde{\nu}$	f	$\tilde{\nu}$	f
1	3609	1.8×10^{-5}	3608	3.7×10^{-5}	3585	1.9×10^{-5}
2	7058	6.1×10^{-7}	7060	1.3×10^{-6}	7014	6.1×10^{-7}
3	10348	1.8×10^{-8}	10356	3.5×10^{-8}	10287	1.8×10^{-8}
4	13478	1.0×10^{-9}	13496	1.9×10^{-9}	13405	1.1×10^{-9}
5	16448	9.2×10^{-11}	16481	1.7×10^{-10}	16367	8.8×10^{-11}

^a Calculated with experimental local mode parameters and a CCSD(T)/aug-cc-pV(T+d)Z dipole moment function. ^b Calculated with experimental local mode parameters and a CCSD(T)/aug-cc-pV(D+d)Z dipole moment function.

the literature; hence, we had to extrapolate the vapor pressure to the temperature at which spectra were recorded (294 K).⁴⁶ It is likely that the low observed oscillator strengths for $\text{CF}_3\text{SO}_3\text{H}$ are due to an overestimate of the vapor pressure of the sample in our cell at 294 K.

The observed local mode parameters, $\tilde{\omega}$ and $\tilde{\omega}x$, of the OH bonds in $\text{CH}_3\text{SO}_3\text{H}$, H_2SO_4 , and $\text{CF}_3\text{SO}_3\text{H}$ are given in Tables 3 and 4, respectively. For $\text{CH}_3\text{SO}_3\text{H}$ and $\text{CF}_3\text{SO}_3\text{H}$, these parameters were obtained from a Birge–Sponer fit of the $\Delta\nu_{\text{OH}} = 1, 4,$ and 5 experimental OH-stretching transitions.^{11,18} For H_2SO_4 , the $\Delta\nu_{\text{OH}} = 1-5$ transitions were used.^{25,30} The observed local mode frequency $\tilde{\omega}$ of $\text{CH}_3\text{SO}_3\text{H}$ is 5 cm^{-1} higher than that of H_2SO_4 and 28 cm^{-1} higher than that of $\text{CF}_3\text{SO}_3\text{H}$, which supports the idea that as the electronegativity of the substituent increases, the OH-stretching frequency should decrease. It is likely that the frequency of $\text{CH}_3\text{SO}_3\text{H}$ would be even higher without the presence of a weak intramolecular interaction ($\text{S}=\text{O}\cdots\text{HO}$), which is likely to reduce the frequency. For $\text{CH}_3\text{SO}_3\text{H}$, we find the observed anharmonicity $\tilde{\omega}x$ to be 2 cm^{-1} higher than that of H_2SO_4 and $\text{CF}_3\text{SO}_3\text{H}$. As a result of the slightly higher frequency and higher anharmonicity, the OH-stretching wavenumber of $\text{CH}_3\text{SO}_3\text{H}$ is lower than H_2SO_4 in the $\Delta\nu_{\text{OH}} = 4$ and 5 regions.

The CCSD(T) calculated local mode parameters for the OH-stretching vibrations of $\text{CH}_3\text{SO}_3\text{H}$, H_2SO_4 , and $\text{CF}_3\text{SO}_3\text{H}$ are presented in Tables 3 and 4. The cc-pV(D+d)Z calculations overestimate the frequency $\tilde{\omega}$ by $25-35 \text{ cm}^{-1}$ and the anharmonicity $\tilde{\omega}x$ by $3-5 \text{ cm}^{-1}$. The aug-cc-pV(D+d)Z results underestimate $\tilde{\omega}$ by $5-15 \text{ cm}^{-1}$ and overestimate $\tilde{\omega}x$ by $6-8 \text{ cm}^{-1}$. For $\text{CH}_3\text{SO}_3\text{H}$ and H_2SO_4 , the frequencies $\tilde{\omega}$ obtained with the aug-cc-pV(T+d)Z basis are overestimated by $\sim 15 \text{ cm}^{-1}$ and the anharmonicities by less than 2 cm^{-1} . These errors are similar to previous calculations at this level and suggest that our experimental local mode parameters are reasonable.⁴⁹

In Table 5, we present the anharmonic oscillator OH-stretching wavenumbers and intensities for $\text{CH}_3\text{SO}_3\text{H}$, H_2SO_4 , and $\text{CF}_3\text{SO}_3\text{H}$ calculated with experimental local mode param-

eters and ab initio dipole moment functions. For $\text{CH}_3\text{SO}_3\text{H}$ and H_2SO_4 , we have used dipole moment functions calculated with the CCSD(T)/AV(T+d)Z method. As mentioned earlier, calculations of $\text{CF}_3\text{SO}_3\text{H}$ with the CCSD(T)/AV(T+d)Z method are computationally prohibitive; hence, for $\text{CF}_3\text{SO}_3\text{H}$ we have used a CCSD(T)/AV(D+d)Z dipole moment function. For $\text{CH}_3\text{SO}_3\text{H}$ and H_2SO_4 , we find calculated oscillator strengths using the aug-cc-pV(D+d)Z and aug-cc-pV(T+d)Z dipole moment functions to differ by less than 10%. The agreement between the calculated and experimental wavenumbers is excellent and supports our modeling of the OH-stretching vibrations as isolated local modes described by Morse oscillators. The anharmonic oscillator local mode model has previously shown to be successful in the calculation of absolute intensities of OH-stretching overtones. For $\Delta\nu_{\text{OH}} = 1$ and 2, the calculated oscillator strength of H_2SO_4 is in excellent agreement with experiment and is within error of the observed intensities.²⁵ For the higher overtones, the agreement is also good, although the calculated intensities are slightly below the lower limits of the observed intensities.^{25,30} Not surprisingly, the calculated oscillator strength of H_2SO_4 is approximately twice that of $\text{CH}_3\text{SO}_3\text{H}$ and $\text{CF}_3\text{SO}_3\text{H}$. If we compare the intensity of a single OH oscillator in each of the sulfonic acids, we find the calculated oscillator strengths to vary by no more than 5%. In the fundamental region, the calculated oscillator strength of $\text{CH}_3\text{SO}_3\text{H}$ is $\sim 40\%$ higher than the experimentally determined intensity.¹¹ The calculated oscillator strength of $\text{CH}_3\text{SO}_3\text{H}$ in the $\Delta\nu_{\text{OH}} = 4-5$ regions is in good agreement with experiment and is within error of the observed intensities. The calculated oscillator strength of $\text{CF}_3\text{SO}_3\text{H}$ is significantly higher than the experimentally determined intensity in the $\Delta\nu_{\text{OH}} = 4$ and 5 regions. As discussed earlier, this discrepancy is probably due to an overestimate of the vapor pressure of $\text{CF}_3\text{SO}_3\text{H}$ in our cell. We can estimate the vapor pressure of $\text{CF}_3\text{SO}_3\text{H}$ using the experimental integrated intensity (cm^{-2}) and our calculated oscillator strengths. For the $\Delta\nu_{\text{OH}} = 4$ and 5 transitions, we derive a vapor pressure of 0.13 and 0.19 Torr, respectively. These values are likely to be slightly overestimated given our calculated oscillator strengths for H_2SO_4 and $\text{CH}_3\text{SO}_3\text{H}$ are $\sim 30\%$ lower than the absolute experimental values for the $\Delta\nu_{\text{OH}} = 4$ and 5 transitions. Taking this correction into account, we estimate the vapor pressure of $\text{CF}_3\text{SO}_3\text{H}$ in our cell to be around 0.1 Torr at 294 K. This value is an order of magnitude smaller than the extrapolated literature value of 1.1 Torr at 294 K.⁴⁶

Conclusions

We have measured the vapor-phase OH-stretching overtone spectra of methanesulfonic acid and trifluoromethanesulfonic acid in the $\Delta\nu_{\text{OH}} = 4$ and 5 regions using cavity ring-down spectroscopy. Comparison of these spectra to our previous work on H_2SO_4 suggests that as the electronegativity of R increases ($\text{CH}_3 < \text{OH} < \text{CF}_3$), the frequency of the OH-stretching mode decreases. In methanesulfonic acid, the anharmonicity of the OH-stretching mode is greater, such that in the $\Delta\nu_{\text{OH}} = 4$ and 5 regions the OH-stretching wavenumber of $\text{CH}_3\text{SO}_3\text{H}$ is lower than H_2SO_4 .

High level ab initio and density functional theory calculations were performed to supplement the spectra. The geometry optimizations show the OH group of $\text{CH}_3\text{SO}_3\text{H}$ is better aligned with the adjacent S=O group than in H_2SO_4 and $\text{CF}_3\text{SO}_3\text{H}$ allowing a more favorable intramolecular interaction (S=O \cdots HO). We have calculated the OH-stretching wavenumbers and intensities using the anharmonic oscillator local mode model with experimental local mode parameters and CCSD(T) ab initio dipole moment functions.

Acknowledgment. We thank D. L. Howard for helpful discussions. J.R.L. is grateful to the Foundation for Research, Science and Technology for a Bright Futures scholarship. We acknowledge the Lasers and Applications Research Theme at the University of Otago for use of their computer facilities. We acknowledge the Marsden Fund administered by the Royal Society of New Zealand, the U.S. National Science Foundation, and CIRES at the University of Colorado, Boulder, for financial support.

Supporting Information Available: The B3LYP/AV-(T+d)Z, CCSD(T)/AV(D+d)Z, and CCSD(T)/AV(T+d)Z geometries for $\text{CH}_3\text{SO}_3\text{H}$ in Z-matrix format; the B3LYP/AV(T+d)Z, CCSD(T)/AV(D+d)Z, CCSD(T)/AV(T+d)Z, and experimental geometries for H_2SO_4 in Z-matrix format; the B3LYP/AV(T+d)Z, CCSD(T)/AV(D+d)Z, and experimental geometries for $\text{CF}_3\text{SO}_3\text{H}$ in Z-matrix format; harmonic normal-mode frequencies and intensities for $\text{CH}_3\text{SO}_3\text{H}$, H_2SO_4 , and $\text{CF}_3\text{SO}_3\text{H}$ calculated with the B3LYP/AV(T+d)Z method. This material is available free of charge via the Internet at <http://pubs.acs.org>.

References and Notes

- (1) Charlson, R. J.; Anderson, T. L.; McDuff, R. E. *Earth System Science*; Academic Press: New York, 2000.
- (2) Warneck, P. *Chemistry of the Natural Atmosphere*, 2nd ed.; Academic Press: San Diego, CA, 2000.
- (3) Donaldson, D. J.; Tuck, A. F.; Vaida, V. *Chem. Rev.* **2003**, *103*, 4717–4730.
- (4) Vaida, V.; Kjaergaard, H. G.; Hintze, P. E.; Donaldson, D. J. *Science* **2003**, *299*, 1566.
- (5) Mills, M. J.; Toon, O. B.; Vaida, V.; Hintze, P. E.; Kjaergaard, H. G.; Schofield, D. P.; Robinson, T. W. *J. Geophys. Res., D: Atmos.* **2005**, *110*, D08201.
- (6) Charlson, R. J.; Lovelock, J. E.; Andreae, M. O.; Warren, S. G. *Nature* **1987**, *326*, 655–661.
- (7) Castebrunet, H.; Genthon, C.; Martinerie, P. *Geophys. Res. Lett.* **2006**, *33*, 22711.
- (8) Kloster, S.; Feichter, J.; Maier-Reimer, E.; Six, K. D.; Stier, P.; Wetzel, P. *Biogeosciences* **2006**, *3*, 29–51.
- (9) Chackalackal, S. M.; Stafford, F. E. *J. Am. Chem. Soc.* **1966**, *88*, 4815–4819.
- (10) Niki, H.; Maker, P. D.; Savage, C. M.; Breitenbach, L. R. *Int. J. Chem. Kinet.* **1983**, *15*, 647–654.
- (11) Mihalopoulos, N.; Barnes, I.; Becker, K. H. *Atmos. Environ.* **1992**, *26A*, 807–812.
- (12) Givan, A.; Loewenschuss, A.; Nielsen, C. J. *J. Mol. Struct.* **2005**, *748*, 77–90.
- (13) Allen, H. C.; Raymond, E. A.; Richmond, G. L. *J. Phys. Chem. A* **2001**, *105*, 1649–1655.
- (14) Durig, J. R.; Zhou, L.; Schwartz, T.; Gounev, T. *J. Raman Spectrosc.* **2000**, *31*, 193–202.
- (15) Bencivenni, L.; Caminiti, R.; Feltrin, A.; Ramondo, F.; Sadun, C. *J. Mol. Struct.* **1992**, *257*, 369–403.
- (16) Wang, L.; Zhang, J. *J. Mol. Struct.* **2002**, *581*, 129–138.
- (17) Balicheva, T. G.; Ligus, V. I.; Fialkov, Y. Y. *Russ. J. Inorg. Chem.* **1973**, *18*, 1701.
- (18) Varetti, E. L. *Spectrochim. Acta* **1988**, *44A*, 733–738.
- (19) Schultz, G.; Hargittai, I.; Seip, R. Z. *Naturforsch.* **1981**, *36A*, 917.
- (20) Delaplane, R. G.; Lundgren, J. O.; Olovsson, I. *Acta. Crystallogr., Sect. B* **1975**, *31*, 2208–2213.
- (21) Otto, A. H.; Steiger, T.; Schrader, S. *J. Mol. Struct.* **1998**, *471*, 105–113.
- (22) Fernandez, L. E.; Altabef, A. B.; Varetti, E. L. *J. Mol. Struct.* **2002**, *612*, 1–11.
- (23) Chackalackal, S. M.; Stafford, F. E. *J. Am. Chem. Soc.* **1966**, *88*, 723–728.
- (24) Stopperka, K.; Kilz, F. Z. *Anorg. Allg. Chem.* **1969**, *370*, 49–58.
- (25) Hintze, P. E.; Kjaergaard, H. G.; Vaida, V.; Burkholder, J. B. *J. Phys. Chem. A* **2003**, *107*, 1112–1118.
- (26) Havey, D.; Feierabend, K.; Vaida, V. *J. Mol. Struct.* **2004**, *680*, 243–247.
- (27) Hintze, P. E.; Feierabend, K. J.; Havey, D. K.; Vaida, V. *Spectrochim. Acta, Part A* **2005**, *61*, 559–566.
- (28) Vaida, V. *Int. J. Photoenergy* **2005**, *7*, 61–70.

- (29) Miller, Y.; Gerber, R. B. *J. Am. Chem. Soc.* **2006**, *128*, 9594–9595.
- (30) Feierabend, K. J.; Havey, D. K.; Brown, S. S.; Vaida, V. *Chem. Phys. Lett.* **2006**, *420*, 438–442.
- (31) Kuczowski, R. L.; Suenram, R. D.; Lovas, F. J. *J. Am. Chem. Soc.* **1981**, *103*, 2561–2566.
- (32) Miller, Y.; Chaban, G. M.; Gerber, R. B. *J. Phys. Chem. A* **2005**, *109*, 6565–6574.
- (33) Henry, B. R. *Acc. Chem. Res.* **1987**, *20*, 429–435.
- (34) Henry, B. R.; Kjaergaard, H. G. *Can. J. Chem.* **2002**, *80*, 1635–1642.
- (35) Henry, B. R. *Acc. Chem. Res.* **1977**, *10*, 207–213.
- (36) Mortensen, O. S.; Henry, B. R.; Mohammadi, M. A. *J. Chem. Phys.* **1981**, *75*, 4800–4808.
- (37) Child, M. S.; Lawton, R. T. *Faraday Discuss.* **1981**, *71*, 273–285.
- (38) Kjaergaard, H. G.; Henry, B. R. *J. Chem. Phys.* **1992**, *96*, 4841–4851.
- (39) Kjaergaard, H. G.; Yu, H.; Schattka, B. J.; Henry, B. R.; Tarr, A. W. *J. Chem. Phys.* **1990**, *93*, 6239–6248.
- (40) Phillips, J. A.; Orlando, J. J.; Tyndall, G. S.; Vaida, V. *Chem. Phys. Lett.* **1998**, *296*, 377–383.
- (41) Donaldson, D. J.; Orlando, J.; Amann, S.; Tyndall, G.; Proos, R.; Henry, B.; Vaida, V. *J. Phys. Chem. A* **1998**, *102*, 5171–5174.
- (42) Brown, S. S.; Wilson, R. W.; Ravishankara, A. R. *J. Phys. Chem. A* **2000**, *104*, 4976–4983.
- (43) Rong, Z.; Henry, B. R.; Robinson, T. W.; Kjaergaard, H. G. *J. Phys. Chem. A* **2005**, *109*, 1033–1041.
- (44) Havey, D. K.; Feierabend, K. J.; Takahashi, K.; Skodje, R. T.; Vaida, V. *J. Phys. Chem. A* **2006**, *110*, 6439–6446.
- (45) Tang, I. N.; Munkelwitz, H. R. *J. Colloid Interface Sci.* **1991**, *141*, 109–118.
- (46) Lamanna, W. M.; Kessel, C. R.; Savu, P. M.; Cheburkov, Y.; Brinduse, S.; Kestner, T. A.; Lillquist, G. J.; Parent, M. J.; Moorhouse, K. S.; Zhang, Y.; Birznies, G.; Kruger, T.; Pallazzotto, M. C. *Adv. Resist Technol. Process. XIX* **2002**, *4690*, 817–828.
- (47) Rothman, L. S.; Jacquemart, D.; Barbe, A.; Benner, D. C.; Birk, M.; Brown, L. R.; Carleer, M. R.; Chackerian, C.; Chance, K.; Coudert, L. H.; Dana, V.; Devi, V. M.; Flaud, J.-M.; Gamache, R. R.; Goldman, A.; Hartman, J.-M.; Jucks, K. W.; Maki, A. G.; Mandin, J.-Y.; Massie, S. T.; Orphal, J.; Perrin, A.; Rinsland, C. P.; Smith, M. A. H.; Tennyson, J.; Tolchenov, R. N.; Toth, R. A.; Vander Auwera, J.; Varanasi, P.; Wagner, G. *J. Quant. Spectrosc. Radiat. Transfer* **2005**, *96*, 139–204.
- (48) Herzberg, G. *Molecular Spectra and Molecular Structure I. Spectra of Diatomic Molecules*, 2nd ed.; D. Van Nostrand Company, Inc.: New York, 1950.
- (49) Howard, D. L.; Jørgensen, P.; Kjaergaard, H. G. *J. Am. Chem. Soc.* **2005**, *127*, 17096–17103.
- (50) Low, G. R.; Kjaergaard, H. G. *J. Chem. Phys.* **1999**, *110*, 9104–9115.
- (51) Atkins, P. W.; Friedman, R. S. *Molecular Quantum Mechanics*, 3rd ed.; Oxford University Press: Oxford, U.K., 1997.
- (52) Rong, Z.; Cavagnat, D.; Lespade, L. In *Lecture Notes in Computer Science*; Sloot, P., Ed.; Springer-Verlag: Berlin, 2003; Vol. 2658, pp 350–356.
- (53) Wilson, A. K.; Peterson, K. A.; Dunning, T. H. *J. Chem. Phys.* **2001**, *114*, 9244.
- (54) Wilson, A. K.; Dunning, T. H., Jr. *J. Chem. Phys.* **2003**, *119* (22), 11712.
- (55) Amos, R. D.; Bernhardsson, A.; Berning, A.; Celani, P.; Cooper, D. L.; Deegan, M. J. O.; Dobbyn, A. J.; Eckert, F.; Hampel, C.; Hetzer, G.; Knowles, P. J.; Korona, T.; Lindh, R.; Lloyd, A. W.; McNicholas, S. J.; Manby, F. R.; Meyer, W.; Mura, M. E.; Nicklass, A.; Palmieri, P.; Pitzer, R.; Rauhut, G.; Schütz, M.; Schumann, U.; Stoll, H.; Stone, A. J.; Tarroni, R.; Thorsteinsson, T.; Werner, H.-J. *MOLPRO A Package of ab Initio Programs*, version 2002.1; University College Cardiff Consultants Limited: Wales, U.K., 2002.
- (56) Ishiuchi, S.; Fujii, M.; Robinson, T. W.; Miller, B. J.; Kjaergaard, H. G. *J. Phys. Chem. A* **2006**, *110*, 7345–7354.
- (57) Bicerano, J.; Schaefer, H. F.; Miller, W. H. *J. Am. Chem. Soc.* **1983**, *105*, 2550–2553.
- (58) Rios, M. A.; Rodriguez, J. *Can. J. Chem.* **1991**, *69*, 201–204.
- (59) Rong, Z.; Howard, D. L.; Kjaergaard, H. G. *J. Phys. Chem. A* **2003**, *107*, 4607–4611.